Phosphorylated-calix[4]arene double-deckers of single rare earth metal ions

COMMUNICATION

Phosphorylated-calix[4]arene double-deckers of single rare earth metal ions†

That's my thinkingReceived 00th January 20xx,
Accepted 00th January 20xx

DOI: 10.1039/x0xx00000x

Marjan Hosseinzadeh,‡*[a] Sergio Sanz,‡[b,c] Jan van Leusen,[a] Natalya V. Izarova,[a,b] Euan K. Brechin,*[d] Scott J. Dalgarno*[e] and Paul Kögerler*[a,b,c]

Combination of phosphoryl and calix[4]arene moieties in the same organic framework (L_{PO}) directs the formation of homoleptic double-decker complexes $[Ln^{III}(L_{PO})_2](O_3SCF_3)_3$ for Ln = Tb and Dy, with the latter displaying slow relaxation of the magnetisation.

p-tert-Butylcalix[4]arene (TBC[4]) is a cone-shaped molecule comprising four phenol units linked by methylene groups.[1] The poly-phenolic nature of the lower-rim presents it as an excellent candidate for metal complexation and it has been successfully employed to create a library of polynuclear complexes with transition metals (TM),[2] lanthanides (Ln)[3] and TM-Ln mixtures (Fig. 1a).[4] The design of mononuclear complexes has received less attention and has mainly focused on TM, although a small number of Ln-based compounds have been synthesised to investigate luminescence,[5] metal extraction,[6] synthetic methodology[7] and magnetic properties.[8] The isolation of a single lanthanide ion with TBC[4] typically requires the alkylation of the four phenolic O-atom positions, or methylation of the distal 1,3-phenolic sites to limit the bridging nature of the ligand.[9] This latter route has been used to investigate the spin dynamics of magnetically anisotropic Ln centres. For example, a combination of *p-tert*-butylcalix[4](OMe)$_2$(OH)$_2$arene (HL) with a Kläui tripodal (L_{OEt}) ligand resulted in a seven-coordinate dysprosium ion in the complex $[Dy^{III}(L)(L_{OEt})]$ (Fig. 1b), which acted as a single-ion magnet (SIM). The ability of the Kläui ligand ($\{(C_5H_5)Co[(RO)_2PO]_3\}^-$, commonly R = Me, Et)[10] to coordinate to TM ions (232 complexes in Cambridge Structural Database) and Ln ions (132 hits) via a facial κ^3-ligand (P=O) hinted at the potential of converting TBC[4] into a tetradentate κ^4-TBC[4] unit towards Ln and/or TM centres through the (RO)$_2$P=O groups. Indeed, TBC[4] derivatised with four diethoxyphosphoryl groups at the lower-rim has been used as a solvent-extraction agent for lanthanum metal.[11] The lanthanum ion is sandwiched between two tetrakis-*O*-(diethoxyphosphoryl)-*p-tert*-butylcalix[4]arene (= L_{PO}) ligands and adopts an eight-coordinate, square-antiprismatic O_8 environment. Sandwich-type complexes of *f*-elements (most commonly Tb and Dy) often display slow relaxation of the magnetisation when the molecular symmetry
is close to D_{4d}[12] and are investigated as materials for potential applications in quantum technologies and molecular spintronics.[13]

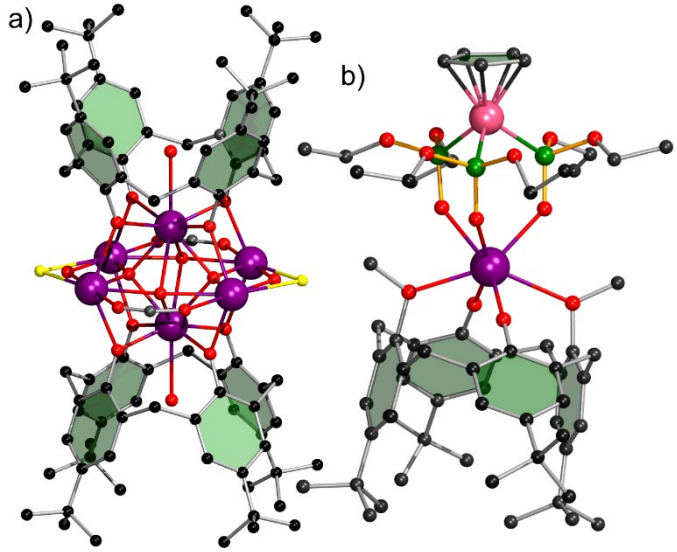

Figure 1. Examples of polynuclear and mononuclear complexes of TBC[4] with Ln ions. a) $[Tb^{III}_6(TBC[4])_2O_2(OH)_{3.32}Cl_{0.68}(HCO_2)_2(dmf)_8(H_2O)_{0.5}]$, b) $[Tb^{III}(TBC[4](OMe)_2(OH)_2)(L_{OEt})]$. Colour code: Tb: purple, O: red, Co: magenta, P: green, Cl: yellow, C: black. C–C/C–O

[a] Institute of Inorganic Chemistry, RWTH Aachen University, 52056 Aachen, Germany. E-mail: paul.koegerler@ac.rwth-aachen.de marjan.hosseinzadeh@ac.rwth-aachen.de
[b] Peter Grünberg Institute, Electronic Properties (PGI-6), Forschungszentrum Jülich, 52425 Jülich, Germany.
[c] Jülich-Aachen Research Alliance, Fundamentals for Future Information Technology (JARA-FIT), Forschungszentrum Jülich, 52425 Jülich, Germany.
[d] EaStCHEM School of Chemistry, The University of Edinburgh, David Brewster Road, Edinburgh, EH9 3FJ, UK. E-mail: ebrechin@ed.ac.uk
[e] Institute of Chemical Sciences, Heriot-Watt University, Riccarton, Edinburgh, EH144AS, UK. E-mail: S.J.Dalgarno@hw.ac.uk

† Electronic Supplementary Information (ESI) available: Synthesis, structural details, magnetic studies related to the discussion of results and additional figures. See DOI: 10.1039/x0xx00000x.

‡Marjan Hosseinzadeh and Sergio Sanz contributed equally to this work.

bonds: grey, P–O: orange, coordinative bonds: two-coloured. H atoms and terminal dmf molecules coordinated to the equatorial terbium atoms in (a) are omitted for clarity.

No other structures with this charge-neutral ligand have been reported, reinvigorating our interest in exploiting it towards metal complexation with paramagnetic rare earth metals.

Herein, we describe the synthesis and characterisation of a new family of homoleptic double-decker species of formula $[M^{III}(L_{PO})_2](OTf)_3$ (M = Y (**1**), Dy (**2**), Tb (**3**); OTf = trifluoromethanesulfonate). Although magnetic TBC[4]-based double-decker complexes are known within polynuclear Ln chemistry, this study represents the first example of the isolation and characterisation of monometallic complexes. Complexes **1** – **3** were synthesised by reacting L_{PO} with $M(OTf)_3$ (stoichiometry 2:1) in dry CH_3CN at ambient temperature for 12 hours. The reaction mixture was filtered to remove any unreacted species and the filtrate was then evaporated under reduced pressure to obtain a white powder. Slow diffusion of Et_2O into a concentrated $CHCl_3$ solution of each complex provided colourless crystals of **1** – **3** in high yields (~70%) and purity (see experimental section in ESI†).

Initially, we explored the reaction conditions in the synthesis of the diamagnetic yttrium complex **1**, $[Y^{III}(L_{PO})_2](OTf)_3$, by ^{31}P and ^{1}H NMR to access the more complicated paramagnetic analogues **2** and **3**. The ^{31}P NMR (162 MHz, CD_3CN) of **1** displays a large upfield shift of ~10.53 ppm, in comparison to uncoordinated L_{PO}, with singlets at –15.04 and –15.10 ppm, corresponding to symmetrically equivalent P^V centres of the diethoxyphosphoryl groups (Fig. S1). Upon coordination, L_{PO} presents two broad singlets of equal intensity at 3.98 and 4.44 ppm in the ^{1}H NMR (400 MHz, CD_3CN) spectrum arising from the preferred orientations of the methylene groups ($POCH_2CH_3$), while the more distant methyl protons remain relatively unchanged. Resonances of the diastereotopic methylene bridge protons located in the *axial* and *equatorial* positions exhibit a downfield shift of 0.12 ppm and 0.26.ppm, respectively, with doublets at 4.98 ppm (CH_{2ax}) and 3.66 ppm (CH_{2eq}), revealing

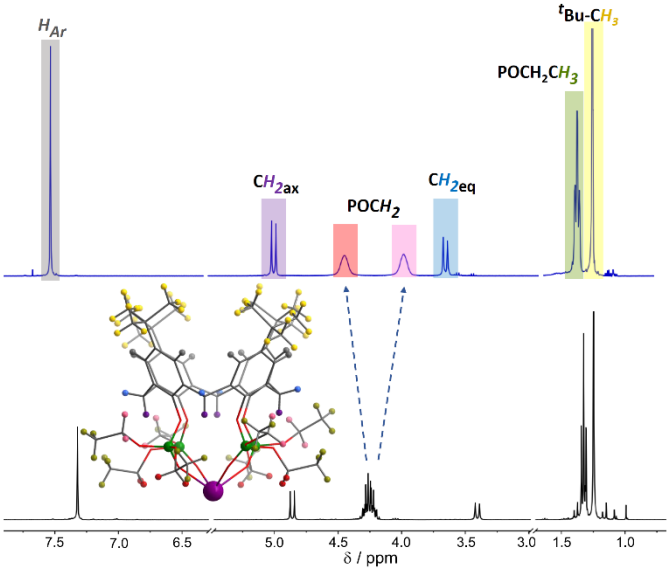

Figure 2. ^{1}H NMR spectra (400 MHz, 300 K) in CD_3CN of **(top)** $[Y^{III}(L_{PO})_2](OTf)_3$ (**1**); **(bottom)** L_{PO} = tetrakis-O-(diethoxyphosphoryl)-*p-tert*-butylcalix[4]arene. Inset: representation of the different hydrogen atoms in $[Y^{III}$(tetrakis-O-(diethoxyphosphoryl)-*p-tert*-butylcalix[4]arene)$]^{3+}$ observable by ^{1}H NMR. Colour code: H–aromatics = grey, H–CH_2axial = purple, H–$POCH_2CH_3$ = red and pink, H–CH_2equatorial = blue, H–$POCH_2CH_3$ = green, and H–^{t}Butyl = yellow.

that the *equatorial* protons are more affected by complex formation. The single set of resonances for the aromatic and *tert*-butyl protons corresponds to an overlap of their chemical shifts due to the cone conformation of the calixarene ligand, where the four aromatic groups are symmetry-related (Fig. 2).

Characterisation of $[Y^{III}(L_{PO})_2](OTf)_3$ (**1**) using EA, IR, UV-Vis, ESI-HRMS, powder and single-crystal XRD studies supports the NMR spectroscopy assignments. Subsequently, complexes of **2** and **3** were isolated following a similar synthetic procedure and were fully characterised by analogous techniques (see the experimental section in ESI†).

Compounds **1** – **3** crystallise in triclinic systems and structure solution of **2** was performed in the space group *P*-1; unit cell measurements confirm that **1** – **3** are isostructural, hence we will describe the molecular structure of **2** as a representative example. The two phosphorylated TBC[4]s adopt a cone conformation and bind the Dy^{3+} ion as tetradentate ligands through lower-rim oxygen (P=O) atoms (Dy^{III}–O: 2.361(4)–2.401(5) Å). While the P=O units point inward to coordinate to the dysprosium atom, the flexible ethoxy groups project outwards due to sterics and the trigonal pyramidal geometry of the P^V atom (Fig. 3). The presence of upper-rim ^{t}Bu and lower-rim alkoxide groups provide solubility in common solvents such as CH_2Cl_2, CH_3CN, acetone, THF, MeOH and EtOH, and thus are key for subsequent manipulation of the sample (*e.g.* crystallisation). The four coordinating oxygen atoms of the calixarene are coplanar and define a virtually regular square (O···O: 2.805(6)–2.832(6) Å) that coordinates to the metal atom, which adopts a square-antiprismatic geometry. The rotation of the skew angles (55.27, 34.45, 55.41 and 34.88°) concerning the eclipsed geometry in the $Dy^{III}O_8$ fragment (Fig. 3b) and the 1.07° angle between the upper and lower planes containing the O_4 coordinating pockets provokes the distortion of the square-antiprismatic O_8 environment and loss of local D_{4d} symmetry.

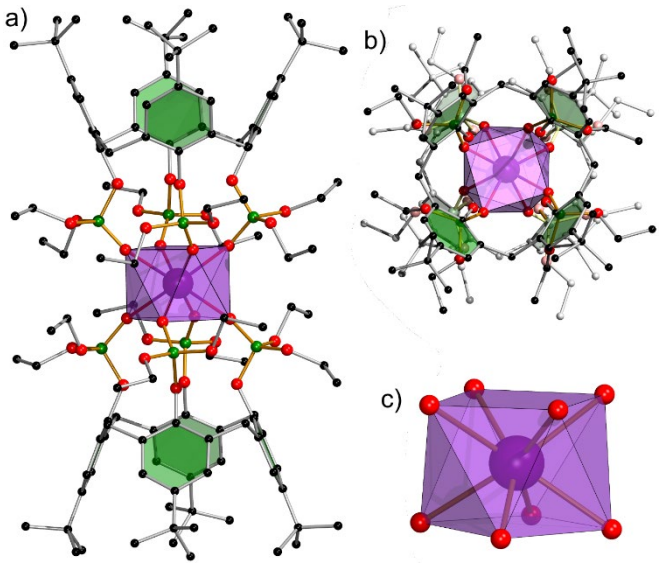

Figure 3. a) Molecular structure of $[Dy^{III}(L_{PO})_2]^{3+}$ in **2**. b) Top view of the molecule along its C_2 axis, showcasing the rotation of the skew angles with respect to the eclipsed geometry in the DyO_8 fragment. The rear L_{PO} ligand is shown in fainter colours. c) The distorted square-antiprismatic $Dy^{III}O_8$ coordination polyhedron (in transparent purple). Colour code as in Fig. 1; Dy^{III}: purple. H atoms and OTf^- anions are omitted for clarity.

Inspection of the crystal packing shows the closest distances at 4.114 Å between neighbouring molecules occurs through $CH_3(^tBu)$–$CH_3(^tBu)$ interactions. Contacts to the nearest counter anions are mediated through $CH_2(OEt)$–$O(OTf^-)$ interactions at 3.253 Å. There are no intra- or intermolecular hydrogen bonds, and the nearest $Dy^{III}\cdots Dy^{III}$ distance is 16.141 Å, effectively isolating the magnetic unit from adjacent clusters (Fig. S4†).

The electronic absorption spectra of **1** – **3** in acetonitrile solution display an intense band at 200 nm and two weak bands at 271 and 280 nm, attributed to (π–π*) transition centred on the phenyl rings of TBC[4] and phosphate moieties (Fig. S5†). FT–IR spectra (Fig. S6,S7†) present vibrations associated with ν(C–H) ~2965–2871 cm^{-1}, ν(arC-C) ~1480 cm^{-1}, ν(P=O) ~1272 and 1240 cm^{-1}, ν(P–OEt) ~1187–1102 cm^{-1}, ν(P–OPh) ~1002–948 cm^{-1} and ν(O–Ph) ~1056 and 1031 cm^{-1}. The presence of two absorption bands at 1272 and 1240 cm^{-1} in the lower wavenumber region compared to the single ν(P=O) stretching band of the precursor L_{PO} at 1275 cm^{-1} indicates the tetradentate nature of the ligand towards the metal centres, as observed by other authors.[14] ESI-HRMS in the positive ion mode for complexes **1** – **3** shows fragmentations characteristic for $[M]^{3+}$ as the most abundant ion, as well as the doubly $[M + OTf]^{2+}$ and singly $[M + 2OTf]^{+}$ charged species, where M = $[M^{III}(L_{PO})_2]$. The isotopic distributions of the experimental data match the calculated species with *m/z* deviations within ~0.001 (Fig. S8–S10†). To investigate the thermal stability of the complexes, thermogravimetric analysis was conducted in an inert atmosphere. All three compounds exhibit thermal stability up to *ca*. 200 °C, wherefrom a ~35% sudden mass loss is observed up to 280 °C, and a more progressive mass decrease (~15%) between 280 and 500 °C that may account for the loss of the three triflate counter anions (Fig. S11†).

The magnetic properties of **2** and **3** in static fields are shown in Fig. 4a as $\chi_m T$ *vs.* *T* plots at 0.1 and 1.0 T. At 290 K, the $\chi_m T$ values are 13.60 (**2**) and 11.88 $cm^3\ K\ mol^{-1}$ (**3**), i.e. within the expected ranges[15] of 13.0 – 14.1 $cm^3\ K\ mol^{-1}$ for Dy^{3+}, and 11.7 – 12.0 $cm^3\ K\ mol^{-1}$ for Tb^{3+}. Upon cooling, the $\chi_m T$ values of both compounds remain almost constant to 100 K, wherefrom they decrease to 10.09 (0.1 T) or 4.93 $cm^3\ K\ mol^{-1}$ (1.0 T) for **2**, and 6.31 (0.1 T) or 3.74 $cm^3\ K\ mol^{-1}$ (1.0 T) for **3** at 2 K. This behaviour is due to the thermal depopulation of the energetically split $2J+1$ m_J substates of the respective ground states ($^6H_{15/2}$ (**2**) and $^7F_6$ (**3**)). Variation at temperatures below 30 K originates from the Zeeman effect that depends on the applied field, and is only marginal at 0.1 T. At 2.0 K the molar magnetisation, M_m, as a function of the applied magnetic field, *B*, rise steeply at low fields (0 to 1 T) and increase progressively to reach 5.6 (**2**) and 5.0 $N_A\,\mu_B$ (**3**) at 5.0 T. These values are approximately half of the saturation values 10 $N_A\,\mu_B$ (**2**) and 9 $N_A\,\mu_B$ (**3**) ($M_{m,sat} = g_J J\ N_A\,\mu_B$) due to the pronounced magnetic anisotropy of each ion.

While complex **3** does not show any frequency-dependent susceptibility signals above 2 K in dynamic magnetic fields, **2** displays weak out-of-phase (χ_m'') signals at zero static magnetic bias field. The signals can be optimally enhanced by application of a 500 Oe static bias field (Fig. 4b); higher bias fields cause increasing contributions of additional relaxation processes.

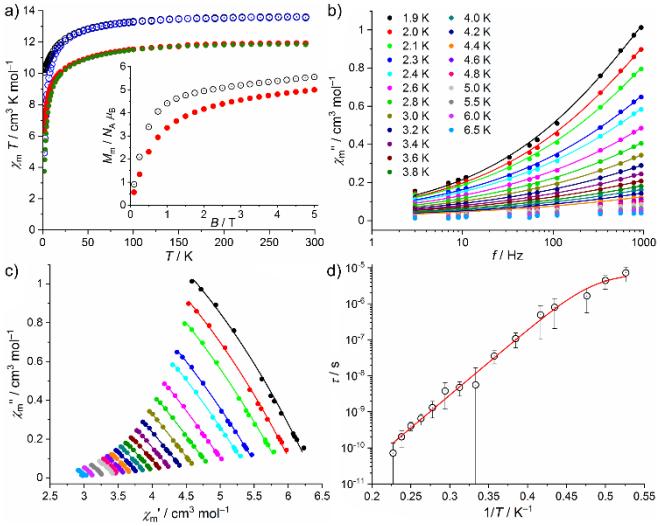

Fig. 4. a) Susceptibility data for **2** and **3** in static magnetic fields: temperature dependence of $\chi_m T$, with data for **2** shown as open black (0.1 T)/blue (1.0 T) circles, for **3** as red (0.1 T)/green (1.0 T) filled circles. Inset: molar magnetisation M_m *vs.* applied magnetic field *B* at 2.0 K (**2**: black open circles, **3**: red filled circles). b-d) Magnetic ac data of **2** at a static bias field of 500 Oe, *T* = 1.9 – 6.5 K. b) Out-of-phase susceptibility χ_m'' *vs.* frequency *f*. c) Cole-Cole plot of χ_m'' *vs.* in-phase χ_m' (filled circles: data, lines: least-squares fits). d) Arrhenius plot of relaxation times τ *vs.* inverse temperature 1/*T*.

Analysing the ac susceptibility data in terms of a generalised Debye expression[16] at each temperature yields fit parameters represented by the solid lines in the Cole-Cole plot (Fig. 4c) and the (χ_m'', χ_m') *vs.* *f* plots (Figs. 4b and S13†). Relaxation times τ are shown in Fig. 4d as τ *vs.* 1/*T*, revealing a distribution α = 0.70±0.07, suggesting the presence of multiple relaxation pathways; we note that α barely changes at higher bias fields. We therefore analysed the data considering Orbach, Raman and direct relaxation processes in tandem with quantum tunnelling of the magnetisation. The best least-squares fit adopts an Orbach and a direct relaxation process represented by the formula $\tau^{-1} = \tau_0^{-1}\exp(-U_{eff}/k_BT) + A_KT$ (k_B: Boltzmann's constant). This yields an attempt time τ_0 = (1.01±0.38)×10^{-14} s, an effective barrier U_{eff} = (29.1±0.9) cm^{-1} for the Orbach process, and the constant A_K = (7.9±2.1)×10^4 $s^{-1}\ K^{-1}$ at 500 Oe static bias field for the direct process. The magnitude of the effective barrier found is in the same range as that observed for structurally comparable compounds, *e.g.* $[Dy^{III}(Pc)_2]^-$ [17] or $[Dy^{III}(PW_{11}O_{39})_2]^{11-}$;[18] however, the attempt time is approximately eight and three orders of magnitude smaller, respectively. The direct process constant A_K is larger than the statistically listed due to the higher margin of error of the points used to determine this value (low *T* points); this does not exert a big influence on the parameters of the Orbach process,

therefore we prefer to use these low *T* points in the fitting procedure rather than ignoring them.

In summary, the combination of phosphoryl and TBC[4] moieties within the same framework affords a ligand capable of forming homoleptic double-decker complexes of formula $[M^{III}(L_{PO})_2](OTf)_3$ in high yields. These compounds actually represent the first examples of magnetic TBC[4]-based mononuclear double-decker structures. The lanthanide ions are eight-coordinate and reside in distorted square-antiprismatic coordination geometries. Ac susceptibility measurements show slow relaxation of the magnetisation for the Dy derivative, which is reproduced best when considering Orbach and direct relaxation processes. Entry into the lanthanide chemistry with this ligand is especially interesting due to the possibility of fine-tuning the coordination sphere and ligand field through controlled hydrolysis of the phosphate ester bonds by lanthanide ions, potentially leading to fascinating new structures and applications. Our current studies show the stability of L_{PO} in dry solvents, and the feasibility of control over the P-O cleavage in "wet" solvents promises different forms of the ligand and double-decker complexes of disparate nuclearity. These results will be communicated in due course and may lead to a better understanding of the magneto-structural relationship.

Conflicts of Interest

There are no conflicts to declare.

Acknowledgements

Marjan Hosseinzadeh gratefully acknowledges financial support by the Alexander von Humboldt Foundation (AvH).

Notes and references

1 C. D. Gutsche, *Calixarenes 2001*, Kluwer Academic Publishers, 2001.

2 (a) S. M. Taylor, J. M. Frost, R. McLellan, R. D. McIntosh, E. K. Brechin and S. J. Dalgarno, *CrystEngComm*, 2014, **16**, 8098–8101; (b) S. M. Taylor, G. Karotsis, R. D. McIntosh, S. Kennedy, S. J. Teat, C. M. Beavers, W. Wernsdorfer, S. Piligkos, S. J. Dalgarno and E. K. Brechin, *Chem. Eur. J.*, 2011, **17**, 7521–7530; (c) S. M. Taylor, R. D. McIntosh, C. M. Beavers, S. J. Teat, S. Piligkos, S. J. Dalgarno and E. K. Brechin, *Chem. Commun.*, 2011, **47**, 1440–1442; (d) G. Karotsis, S. J. Teat, W. Wernsdorfer, S. Piligkos, S. J. Dalgarno and E. K. Brechin, *Angew. Chem., Int. Ed.*, 2009, **48**, 8285–8288; (e) M. Coletta, S. Sanz, E. K. Brechin and S. J. Dalgarno, *Dalton Trans.*, 2020, **49**, 9882–9887; (f) M. Coletta, S. Sanz, L. J. McCormick, S. J. Teat, E. K. Brechin and S. J. Dalgarno, *Dalton Trans.*, 2017, **46**, 16807–16811; (g) R. McLellan, M. A. Palacios, S. Sanz, E. K. Brechin and S. J. Dalgarno, *Inorg. Chem.*, 2017, **56**, 10044–10053.

3 (a) S. Sanz, R. D. Mc Intosh, C. M. Beavers, S. J. Teat, M. Evangelisti, E. K. Brechin and S. J. Dalgarno, *Chem. Commun.*, 2012, **48**, 1449–1451; (b) Y. Bi, G. Xu, W. Liao, S. Du, R. Deng and B. Wang, *Sci. China Chem.*, 2012, **55**, 967–972.

4 (a) G. Karotsis, S. Kennedy, S. J. Teat, C. M. Beavers, D. A. Fowler, J. J. Morales, M. Evangelisti, S. J. Dalgarno and E. K. Brechin, *J. Am. Chem. Soc.*, 2010, **132**, 12983–12990; (b) M. A. Palacios, R. McLellan, C. M. Beavers, S. J. Teat, H. Weihe, S. Piligkos, S. J. Dalgarno and E. K. Brechin, *Chem. Eur. J.*, 2015, **21**, 11212–11218; (c) S. Sanz, K. Ferreira, R. D. McIntosh, S. J. Dalgarno and E. K. Brechin, *Chem. Commun.*, 2011, **47**, 9042–9044.

5 (a) C. R. Driscoll, B. L. Reid, M. J. McIldowie, S. Muzzioli, G. L. Nealon, B. W. Skelton, S. Stagni, D. H. Brown, M. Massi and M. I. Ogden, *Chem. Commun.*, 2011, **47**, 3876–3878; (b) R. S. Viana, C. A. F. Oliveira, J. Chojnacki, B. S. Barros, S. Alves-Jr and J. Kulesza, *J. Solid State Chem.*, 2017, **251**, 26–32; (c) C. R. Driscoll, B. W. Skelton, M. Massi and M. I. Ogden, *Supramol. Chem.*, 2016, **28**, 567–574.

6 (a) P. D. Beer, M. G. B. Drew, A. Grieve, M. Kan, P. B. Leeson, G. Nicholson, M. I. Ogden and G. Williams, *Chem. Commun.*, 1996, **1**, 1117–1118; (b) P. D. Beer, M. G. B. Drew, M. Kan, P. B. Leeson, M. I. Ogden and G. Williams, *Inorg. Chem.*, 1996, **35**, 2202–2211.

7 (a) G. L. Nealon, M. Mocerino, M. I. Ogden and B. W. Skelton, *J. Incl. Phenom. Macrocycl. Chem.*, 2009, **65**, 25–30; (b) P. D. Beer, M. G. B. Drew, P. B. Leeson and M. I. Ogden, *Inorg. Chim. Acta*, 1996, **246**, 133–141; (c) F. Estler, E. Herdtweck and R. Anwander, *J. Chem. Soc., Dalton Trans.*, 2002, **65**, 3088–3089; (d) M. I. Ogden, B. W. Skelton and A. H. White, *C. R. Chimie*, 2005, **8**, 181–187.

8 F. Gao, L. Cui, Y. Song, Y. Z. Li and J. L. Zuo, *Inorg. Chem.*, 2013, **53**, 562–567.

9 See for example (a) M. J. McIldowie, B. W. Skelton, M. Mocerino and M. I. Ogden, *J. Incl. Phenom. Macrocycl. Chem.*, 2015, **82**, 43–46; (b) D. D'Alessio, S. Muzzioli, B. W. Skelton, S. Stagni, M. Massi and M. I. Ogden, *Dalton Trans.*, 2012, **41**, 4736–4739; (c) J. Gottfriedsen, R. Hagner, M. Spoida and Y. Suchorski, *Eur. J. Inorg. Chem.*, 2007, 2288–2295.

10 W. Kläui, *Angew. Chem., Int. Ed.*, 1990, **29**, 627–637.

11 J. M. Harrowfield, M. Mocerino, B. J. Peachey, B. W. Skelton and A. H. White, *J. Chem. Soc., Dalton Trans.*, 1996, 1687–1699.

12 J. L. Liu, Y. C. Chen and M. L. Tong, *Chem. Soc. Rev.*, 2018, **47**, 2431–2453.

13 (a) A. Gaita-Ariño, F. Luis, S. Hill and E. Coronado, *Nat. Chem.*, 2019, **11**, 301–309; (b) E. Moreno-Pineda, C. Godfrin, F. Balestro, W. Wernsdorfer and M. Ruben, *Chem. Soc. Rev.*, 2018, **47**, 501–513; (c) A. Ghirri, A. Candini and M. Affronte, *Magnetochemistry*, 2017, **3**, 12; (d) S. Thiele, F. Balestro, R. Ballou, S. Klyatskaya, M. Ruben and W. Wernsdorfer, *Science*, 2014, **344**, 1135–1138; (e) G. Aromí, D. Aguilà, P. Gamez, F. Luis and O. Roubeau, *Chem. Soc. Rev.*, 2012, **41**, 537–546; (f) A. Cornia, M. Mannini, P. Sainctavit and R. Sessoli, *Chem. Soc. Rev.*, 2011, **40**, 3076–3091; (g) M. Urdampilleta, N. V. Nguyen, J. P. Cleuziou, S. Klyatskaya, M. Ruben and W. Wernsdorfer, *Int. J. Mol. Sci.*, 2011, **12**, 6656–6667; (h) L. Bogani and W. Wernsdorfer, *Nat. Mater.*, 2008, **7**, 179–186.

14 (a) X. Hu, W. Dou, C. Xu, X. Tang, J. Zheng and W. Liu, *Dalton Trans.*, 2011, **40**, 3412–3418; (b) A. M. J. Lees, R. A. Kresinski and A. W. G. Platt, *New J. Chem.*, 2004, **28**, 1457-1463; (c) Z. Hnatejko, S. Lis, G. Pawlicki and G. Meinrath, *J. Alloys Compd.*, 2008, **451**, 395-399.

15 H. Lueken, *Magnetochemie*, Teubner Verlag, Stuttgart, **1999**.

16 K. S. Cole and R. H. Cole, *J. Chem. Phys.*, 1941, **9**, 341–351.

17 N. Ishikawa, M. Sugita, T. Ishikawa, S.-Y. Koshihara and Y. Kaizu, *J. Am. Chem. Soc.*, 2003, **125**, 8694–8695.

18 P. Ma, F. Hu, Y. Huo, D. Zhang, C. Zhang, J. Niu and J. Wang, *Cryst. Growth Des.*, 2017, **17**, 1947–1956.